

Check for updates

www.advmattechnol.de

High-Resolution 3D Printing of Pancreatic Ductal Microanatomy Enabled by Serial Histology

Ashley L. Kiemen,* André Forjaz, Ricardo Sousa, Kyu Sang Han, Ralph H. Hruban, Laura D. Wood, PeiHsun Wu, and Denis Wirtz

Pancreatic ductal adenocarcinoma (PDAC) is a deadly cancer that can develop from pancreatic intraepithelial neoplasia (PanIN), a microscopic lesion in the pancreatic ductal system. PanIN and PDAC are conventionally studied in 2D via histological tissue sections. As such, their true structure is poorly understood due to the inability to image them in 3D. CODA, a recently developed technique for reconstruction of tissues at cellular resolution, is used to study the 3D morphology of the pancreas. Here, CODA is extended through 3D printing of normal pancreatic ducts, PanIN, and PDAC at cm-scale and µm resolution. A methodology is presented to create 3D printable files from anatomical maps generated from serial histological images and to show detailed validation of the accuracy of this method. Existing 3D printing workflows utilizing medical images derived from computerized tomography (CT), X-ray, and magnetic resonance imaging (MRI) are scientifically proven to be useful in printing whole organ-scale structures with sub-mm resolution. Here, using serial histological sections, it is demonstrated that 3D printing of higher-resolution structures is also possible. Finally, with the 3D models of normal ducts, PanIN, and PDAC, marked changes to the structure of the human pancreas during tumorigenesis are revealed.

1. Introduction

Pancreatic ductal adenocarcinoma (PDAC) is one of the deadliest of the solid malignancies and is projected to be the second leading cause of cancer-related deaths by 2030.^[1,2] Pancreatic intraepithelial neoplasias (PanINs) are microscopic precursor lesions to

A. L. Kiemen, R. H. Hruban, L. D. Wood, D. Wirtz Department of Pathology, The Sol Goldman Pancreatic Cancer Research Center

The Johns Hopkins University School of Medicine

Baltimore, MD 21287, USA E-mail: kiemen@jhmi.edu

A. L. Kiemen, R. H. Hruban, L. D. Wood, D. Wirtz Department of Oncology, The Sol Goldman Pancreatic Cancer Research

The Johns Hopkins University School of Medicine Baltimore, MD 21287, USA

A. Forjaz, R. Sousa, K. S. Han, P. Wu, D. Wirtz Department of Chemical & Biomolecular Engineering The Johns Hopkins University 3400 N Charles St., Baltimore, MD 21211, USA

The ORCID identification number(s) for the author(s) of this article can be found under https://doi.org/10.1002/admt.202301837

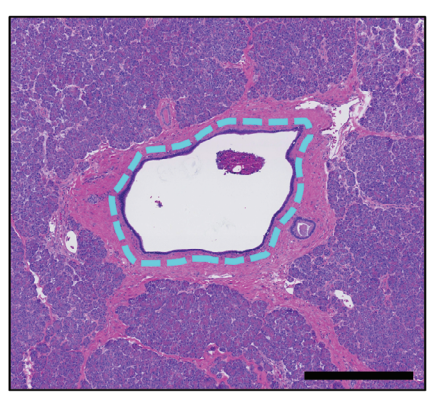
DOI: 10.1002/admt.202301837

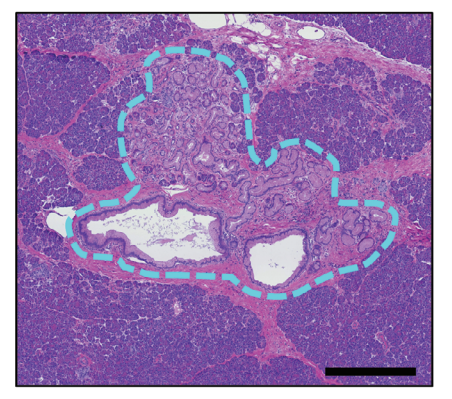
PDAC that inhabit the pancreatic ducts. PanINs are defined as <0.5 cm in their primary dimension and are not classically visible in 3D as they are too small to detect directly via noninvasive imaging techniques such as computerized tomography (CT), endoscopic ultrasound (EUS), or magnetic resonance imaging (MRI).[3] One reason for the deadliness of pancreatic cancer is our inability to effectively screen for microscopic precursor lesions or small, low-stage, PDACs via routine clinical imaging, resulting in late-stage diagnoses where distant metastases are often present.[4,5] Instead, the microanatomy of the normal pancreatic ducts. PanIN lesions. and invasive pancreatic cancer is primarily studied in surgically resected samples cut into 2D hematoxylin and eosin (H&E) stained sections. While H&E allows for high-resolution visualization of pancreatic structure and identification of normal pancreatic ducts, PanINs, and

PDACs for clinical diagnosis, our understanding of these microscopic structures is hindered by this 2D lens (**Figure 1**). Extrapolation of 3D tumor morphology in 2D images is not only difficult but has been shown to affect estimation of tissue composition and the accuracy of clinical grading.^[6,7] Obtaining accurate, 3D views of microanatomical structures is important for improving our understanding of the early stages of pancreatic cancer development.^[5,7–9]

Existing workflows utilize medical images derived from CT, X-ray, MRI, and EUS to 3D print anatomical models of human tissues and have proven to be scientifically and clinically useful.[10-12] 3D printing allows scaling-up of microscopic structures to sizes discernable by the naked eye and scaling-down of excessively large structures to similarly manageable scales. Scientifically, 3D printed models have been created for instructional use in anatomy classes and as templates for bioprinting.[13,14] In the clinic, 3D printed models of tumors have been used to explain complicated surgeries to patients.[11,15] Conventional 3D printing using CT, X-ray, MRI, or tissue clearing enables printing of structures identifiable by their unique nuclear photon or radiographic density, autofluorescence, or labelling by specific antibodies. This allows printing of the macroscopic and mesoscopic structure of whole organs such as the heart, the airways of the lungs, the pancreas, the liver, and the kidneys.[11,12,16,17]

2355790x, 0, Downloaded from https://onlinelibrary.wiley.com/doi/10.1002/admt.202301837 by Johns Hopkins University, Wiley Online Library on [050320224]. See the Terms and Conditions (https://onlinelibrary.wiley.com/terms-and-conditions) on Wiley Online Library for rules of use; OA articles are governed by the applicable Creative Commons Licensen





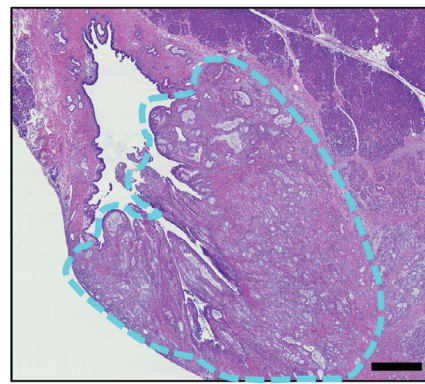


Figure 1. Pancreatic tumorigenesis in histology. Pancreatic cancer develops from PanIN, microscopic precursor lesions in the ductal system of the pancreas. H&E images are provided showing examples of: (left) normal pancreatic ducts, (center) PanIN, and (right) PDAC. Structures of interest outlined in dashed, light-blue. Scale bar = 0.5 mm. Due to the microscopic nature of pancreatic anatomy, these structures are almost universally studied in 2D via histologic imaging.

However, the microscopic size of some pancreatic ducts (as small as 10 μ m in diameter) and our inability to specifically label the normal pancreatic ducts, PanIN, and PDAC in densely fibrotic tissues using antibodies, [9,18,19] hinders our ability to 3D print the pancreatic ductal system using current approaches.

CODA is a recently developed technique that utilizes serial tissue sectioning and deep learning to digitally reconstruct the 3D microanatomy of tissues at single cell resolution.^[20] CODA has revealed striking heterogeneity in the incidence, morphology, and molecular characteristics of PanINs and insights into the 3D nature of PDAC invasion into the adjacent pancreatic parenchyma. [8,20-25] However, the power of CODA in creating accurate, digital 3D reconstructions of tissue is limited by the 2D nature of computer screens—3D anatomical renderings are visualized as 2D images or rotating videos (Video S1, Supporting Information). Here, we present an extension to the CODA technique through which normal pancreatic ducts, PanINs, and PDACs may be accurately 3D printed. These 3D printed pancreatic structures are educationally useful, revealing marked morphological changes to the pancreatic ductal system during tumorigenesis. The proposed workflow shows the utility of using deep learning and serial histological sectioning approaches to create 3D printed models of microscopic tissues that cannot be seen in 3D using other imaging techniques. Below, we describe a workflow through which these digital, 3D tissue maps are converted to µm-resolution 3D-printable files.

2. Experimental Section

2.1. Sample Preparation

The histological images used for 3D reconstructions of human pancreatic tissue used in this project were previously described by Kiemen et al.^[20] This retrospective study was approved by the Johns Hopkins University School of Medicine institutional review board (IRB00164824). Briefly, human pancreas tissues were collected following routine pancreatic resections performed at the Johns Hopkins Hospital in response to diagnosis of pancreatic ductal adenocarcinoma, pancreatic neuroendocrine tumors, or other abnormalities of the pancreas. Samples were forma-

lin fixed, paraffin embedded, serially sectioned at a thickness of $4\,\mu m$, and stained with hematoxylin and eosin (H&E). Here, three cm³-sized samples of human pancreatic tissue were collected, containing non-diseased pancreatic parenchyma, grossly normal pancreatic parenchyma containing pancreatic cancer precursor lesions, and pancreatic tissue containing invasive cancer.

2.2. CODA 3D Reconstruction of Pancreas Tissue

CODA creates digital, labelled volumes of dense tissues using deep learning and image processing applied to serial histological images (**Figure 2**). Here, tissues were formalin-fixed and paraffinembedded, then, serially sectioned, resulting in 1200–1600 sections per sample. Every third section (or every 12 μm) was stained with H&E. Stained tissue sections were digitized at 20× magnification ($\approx 0.5~\mu m$ per pixel) using a Hammamatsu Nanozoomer. Using MATLAB 2022b, the histological images were first downsampled to create pseudo-5× (2 μm per pixel) and pseudo-1.25× (8 μm per pixel) files. Low magnification (pseudo-1.25×) copies of the H&E images were registered using a nonlinear global and elastic image registration pipeline, which was designed to maximize the cross-correlation of serial images. Registration resulted in a stack of continuous H&E images, allowing visualization of 3D pancreatic microanatomy.

In a parallel step, the microanatomical structures of the pancreas were labelled in the pseudo-5× copies of the H&E images using a semantic segmentation algorithm. The model was trained to recognize normal pancreatic ducts, PanINs, PDACs, acinar lobules, islets of Langerhans, vasculature, nerves, stroma, fat, and non-tissue pixels in H&E-stained images of human pancreas. Nine images were extracted from each sample to generate training and testing data. Fifty annotations of each tissue type were annotated per image. Eight images were used for model training and one image was used for independent testing of model accuracy. Additional annotations were made until a per-class precision and recall of 90% was reached. Following model testing, all serial images were segmented at a resolution of two µm per pixel, and segmented images were registered using the displacement fields calculated on the low resolution

2355790x, 0, Downloaded from https://onlinelibrary.wiley.com/doi/10.1002/admt.202301837 by Johns Hopkins University, Wiley Online Library on [050320224]. See the Terms and Conditions (https://onlinelibrary.wiley.com/terms-and-conditions) on Wiley Online Library for rules of use; OA articles are governed by the applicable Creative Commons Licensen

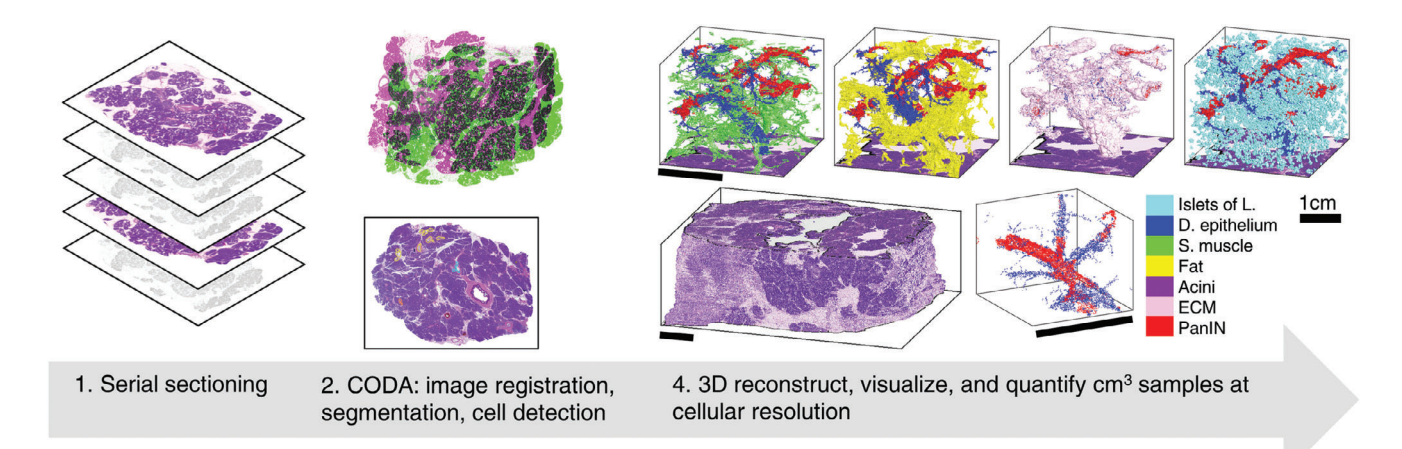


Figure 2. CODA 3D reconstruction of microanatomy from serial histological sections. CODA enables construction of μ m-resolution maps of pancreatic tissues using serial histological sectioning, image registration, deep learning semantic segmentation, and cell detection. Resected tissues are formalin fixed, paraffin embedded, and serial sectioned. Every third section (or every 12 μ m) is stained with hematoxylin and eosin and digitized. Tissue images are registered, and a deep learning semantic segmentation algorithm is used to label microanatomical structures. The resulting labelled maps enable 3D rendering and quantification of tissue microanatomy. Scale bar = 1 cm.

H&E images. Registered, labelled images were loaded into a 3D matrix where they could be visualized and quantified.

Digital 3D renderings were created to visualize the labelled tissues. 3D renderings were created using the "patch" and "isosurface" features in MATLAB. To create the appearance of 3D depth in the renderings, surfaces were plotted within digital 3D space and lighting was cast over the structures to simulate shadows.

2.3. Construction of 3D Printable Files from Serial Histological Data Generated by CODA

CODA creates 3D datasets stored in matrix (M \times N \times Z) format. In order to create 3D-printable files, the following workflow was established. First, the structure of interest (normal pancreatic ducts, PanINs, or invasive pancreatic cancer) was isolated in the pancreatic tissue matrix. These matrix data were converted to triangular mesh format made of vertex triplets and triangle faces and exported in xml files. Due to the large size of the matrices required to print >cm³ sized objects at 12 µm resolution, the authors' desktop memory was not sufficient to reduce the number of vertices in these meshes, resulting in cuboidal meshes and stl files in excess of 3 GB. To reduce the number of points in these meshes while maintaining structure connectivity and morphology, the application zBrush was used. After importing the large stl files into zBrush, the mesh integrity was first checked to fill any holes, delete intersecting faces, and remove duplicate vertices incidentally created during the MATLAB export. Next, a dynamesh was applied to overlay the original 3D mesh, with a resolution of 60%. To reduce the number of vertices of this overlaying mesh, the decimation master was used to remove 95% of created vertices. Finally, these reduced meshes were exported as stl files.

The stl files were loaded into GrabCad print, where they were upsized to 15× biological dimensions. Any noncomplete triangles or missing vertices were filled, and the 3D printer path was determined. To maintain connectivity of delicate pancreatic ductal structures, printing was done with a solid infill and

0.05 in. body thickness. Data were exported in.cmb format and 3D printed in acrylonitrile butadiene styrene (ABS) on a Stratasys F370 printer. ABS was chosen due to its high mechanical strength, elastic modulus, thermoforming properties, and ease of printing along with dissolvable support material. Following printing, the supports were dissolved through immersion in a mild sodium hydroxide solution.

2.4. Validation of 3D Printing Workflow

To quantify the percent change in 3D structure as a result of the authors' file size reduction pipeline, two validation approaches were utilized. First, to determine the extent of morphology change in the 3D models as a result of the smoothing pipeline, the 3D intersection over union (IoU) of pre-versus post- smoothing meshes was calculated. Using the 3D matrix CODA data, 10 000 coordinates known to be contained in the printed structure were randomly sampled. Using the inpolyhedron function,[26] which of these random points were contained within the raw and smoothed 3D meshes was determined. IoU was calculated by taking the ratio of points contained in both meshes to the points contained in either mesh. The second validation approach was to design a digital model with predetermined dimensions. This model was smoothed and printed, and the resulting structure was measured. While the convoluted structure of pancreatic ducts makes them difficult to measure for validation in this project, measurement of the simpler structure of the validation model allowed quantification of the error introduced as a result of conversion from 3D matrix to triangulated mesh, the smoothing of the mesh, and the 3D printing process.

3. Results

Three human pancreas samples containing normal pancreatic ducts, PanINs, and PDACs were identified (Figure 1). CODA

23657978, 0, Downloaded from https://onlinelibrary.wiley.com/doi/10.1002/dmtn.020301837 by Johns Hopkins University, Wiley Online Library on [050520224]. See the Terms and Conditions (https://onlinelibrary.wiley.com/terms-and-conditions) on Wiley Online Library or rules of use; OA arches are governed by the applicable Creative Commons Licensen

Table 1. 3D printing workflow file size reduction and validation of 3D smoothing algorithm. Raw and smoothed 3D mesh file sizes. Calculated intersection over union (IoU) of the raw and smoothed meshes as estimation of loss in morphology.

Model	Original size [MB]	Smoothed size [MB]	% File reduction	IoU [%]
Normal pancreas	2813.7	32.2	98.8	95.8
PanIN	2996.2	63.0	97.9	99.2
PDAC	3037.6	52.9	98.3	99.0
Validation model	1162.4	7.8	99.3	98.5
Mean	2502.5	39.0	98.6	98.1

was used to create digital 3D maps of tissue microanatomy from high-resolution serial, H&E images. Images were transformed into quantifiable, volumetric datasets at $12 \times 12 \times 12 \ \mu m^3$ per voxel resolution through application of a nonlinear image registration algorithm, generation of nuclear coordinates, and deep learning labelling of microanatomy using semantic segmentation (Figure 2). The trained segmentation model was tested on independent histological images and found to label histological components to an accuracy of 96.6%.

We determined that sample A contained only grossly normal pancreatic parenchyma, sample B contained grossly normal pancreatic parenchyma and several large PanIN lesions, and sample C contained a large region of invasive pancreatic cancer adjacent to a grossly normal pancreatic lobule. The reconstructed samples were 1.74, 3.46, and 2.12 cm³ in volume, respectively. We isolated the normal ductal epithelium from sample A, independent PanIN lesions from sample B, and a large region of invasive cancer from sample C for 3D printing. Sample A contained 10.2 mm³ of normal duct within a region of $26.5 \times 19.0 \times 5.5$ mm³. Sample B contained a total of 40.5 mm³ of

PanIN, consisting of several spatially separate lesions. The largest PanIN in the sample (chosen for 3D printing) was 31.7 mm³ and was contained within a region of $15.9 \times 12.6 \times 7.6$ mm³. Sample C contained a region of 30.5 mm³ of invasive pancreatic cancer contained within a region of $12.7 \times 9.2 \times 3.2$ tmm³.

Datasets were converted to 3D meshes and exported in.stl format. These meshes were composed of vertices and triangles that exactly mimicked the voxels of the original 3D matrices. For pancreatic datasets composed of >6 billion voxels, this resulted in cube-like surfaces and.stl file sizes in excess of 3 GB. To smooth the surface of the meshes, we used the software ZBrush. Within ZBrush, we reduced the filesize through creation of a mesh that maintained the original anatomical structure; while, comprising many fewer vertices. We then re-exported the stl files, with an average filesize reduction of 98.6% (Table 1). Exported.stl files were prepared for 3D printing using GrabCad print. Meshes were loaded and rescaled from biological size to 15-times biological size, followed by 3D printing.

Using the proposed workflow, we successfully 3D printed normal pancreatic ducts, PanIN lesions, and PDAC (Figure 3). The 3D printed structures allow clear visualization of changes to pancreatic morphology during tumorigenesis. While the nonneoplastic ductal system appears to follow ordered branching patterns, the 3D printed PanIN lesions show regions of tubular ductal structures interspersed with large, dilated, "balloon-like" regions and solid, lobular-like regions. The 3D printed cancer appears as a near solid mass with distinct regions of invasion projecting into the normal adjacent pancreatic parenchyma.

The function of the exocrine pancreas is to create digestive enzymes in the acinar cells of the pancreatic lobules and to transport these enzymes within the duct system to the duodenum and eventually to the intestines by way of the pancreatic ducts. Pancreatic neoplasms such as PanINs can block the passages of the

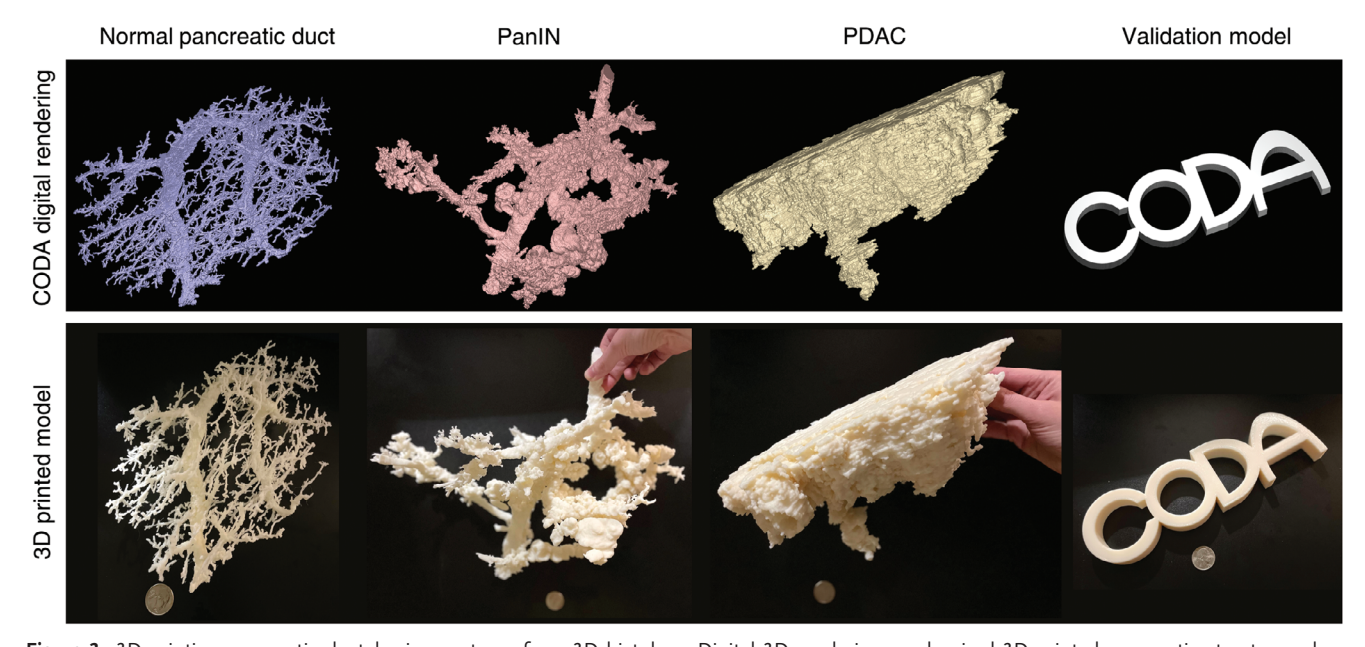


Figure 3. 3D printing pancreatic ductal microanatomy from 3D histology. Digital 3D renderings and paired 3D printed pancreatic structures show complexity of pancreatic architecture. The proposed 3D printing workflow preserves the anatomy present in the digital volumes. From left to right: normal pancreatic ducts, PanIN (cancer precursor lesions), pancreatic cancer, and a workflow validation model. A dime is shown for scale.

2355790x, 0, Downloaded from https://onlinelibrary.wiley.com/doi/10.1002/admt.202301837 by Johns Hopkins University, Wiley Online Library on [050320224]. See the Terms and Conditions (https://onlinelibrary.wiley.com/terms-and-conditions) on Wiley Online Library for rules of use; OA articles are governed by the applicable Creative Commons Licensen

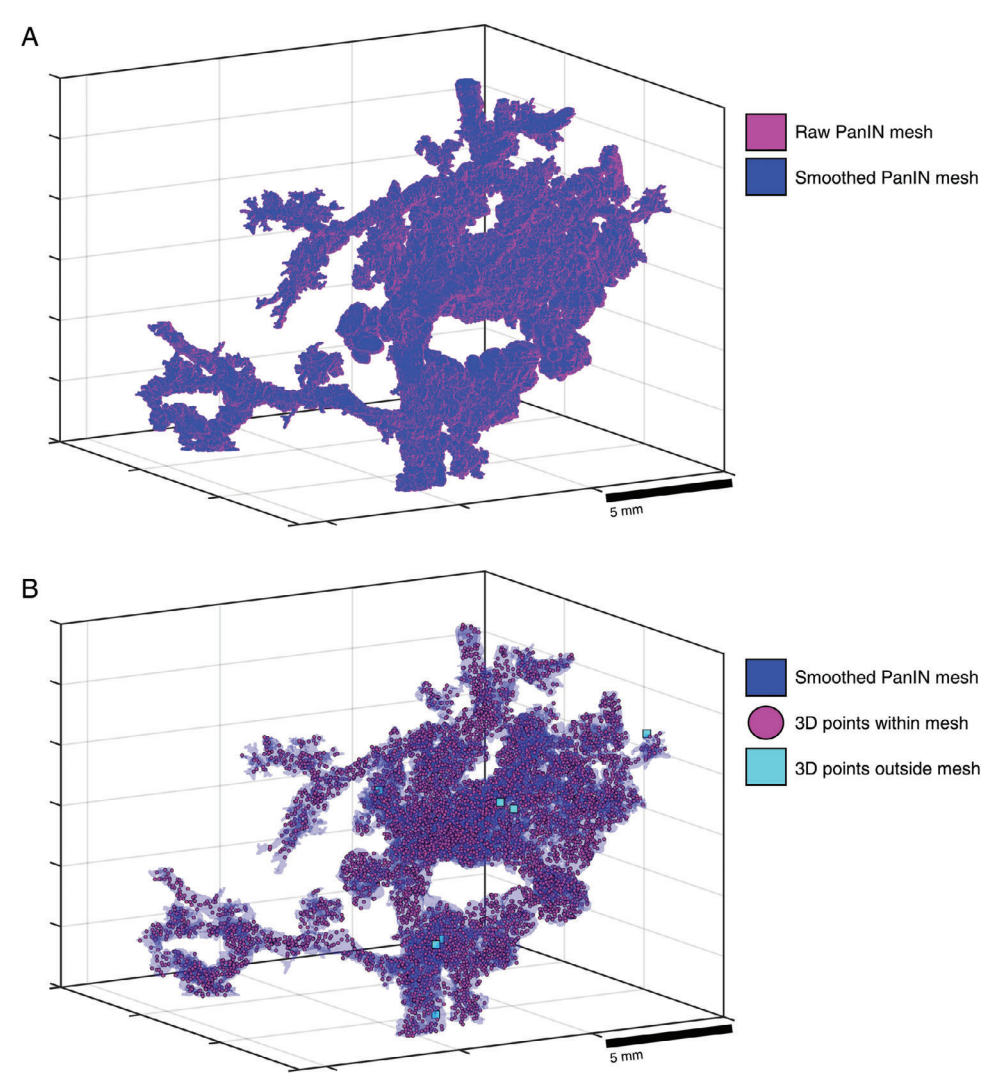


Figure 4. Sample renderings of 3D mesh data used in workflow validation. A) Overlay of raw (pink) and smoothed (blue) meshes. The high concordance of the 3D renders supports that our smoothing algorithm does not greatly alter 3D morphology. B) Overlay of the smoothed mesh used for 3D printing and 10 000 randomly sampled coordinates known to be contained within the original CODA matrix. Round points plotted in pink are determined to fall within the smoothed mesh; while, square points plotted in cyan are determined to lie outside the mesh. These cyan points represent errors introduced by the smoothing algorithm.

pancreatic ducts, resulting in atrophy of the upstream acinar lobules and creating abnormal balloon-like growths in the ducts. Extension of PanIN into regions previously inhabited by the acinar cells (or acinar to ductal metaplasia) can result in regions of solid, lobular PanIN lesions, further disrupting the natural order of the pancreas. As invasive cancer, PDAC further disrupts pancreatic function. In regions near the tumor, there is often total destruction of the exocrine pancreas. Pancreatic cancer often appears as a sparse or solid tumor with many tongues of growth into adjacent tissues along the vasculature, nerves, and aligned stromal fibers. These marked changes are reflected in the 3D printed models. The ordered branching of the normal pancreatic duct model is contrasted by the disordered structure of the PanIN, where ductal branches are interspersed with dilated regions and solid-appearing clusters of cells. Finally, the cancer model resem-

bles a large, solid structure with tentacles of growth extending far from the central mass.

We used two metrics to evaluate the quality of our 3D printing pipeline. First, we evaluated the change in object shape due to the vertex reduction performed in ZBrush using an intersection-over-union calculation (Figure 4). This metric compared the original many-vertex 3D mesh to the reduced filesize 3D mesh to determine the percent loss in structure due to smoothing. Average IoU scores were 98.1%, suggesting that our vertex reduction smoothing workflow preserves 3D pancreatic structure (Table 1). Second, we designed an irregular 3D object with predetermined dimensions and applied our 3D printing pipeline to it in order to evaluate how closely the physical printed shape matched our original design. Measurement of the dimensions of our validation model show 1.16% error (Table 2), suggesting that

23657978, 0, Downloaded from https://onlinelibrary.wiley.com/doi/10.1002/dmtn.020301837 by Johns Hopkins University, Wiley Online Library on [050520224]. See the Terms and Conditions (https://onlinelibrary.wiley.com/terms-and-conditions) on Wiley Online Library or rules of use; OA arches are governed by the applicable Creative Commons Licensen

Table 2. Quantification of error in 3D printing workflow using measurement of "CODA" validation structure. Predicted and measured validation model dimensions and calculated percent error.

	Predicted [cm]	Measured [cm]	Error [%]
Thickness of 'C'	1.20	1.21	0.83
Diameter of 'O'	7.50	7.54	0.53
Height of 'A' center bar	1.20	1.21	1.08
Thickness of structure	2.25	2.30	2.22
-	_	Mean	1.16

the 3D printing process introduces little error into the created biological models.

Compared to existing 3D printing methodologies, our pipeline enables high resolution ($12~\mu m$) printing of mesoscale (mm to cm lengthscale) structures. In addition, 3D printing from serial histological images has the advantage of enabling printing of anatomy that is only identifiable from H&E (such as differentiation of normal, cancer precursor lesions, and invasive cancer cells in the pancreas). Conversely, printing anatomy from diagnostic images such as CT or MRI has the advantage of whole organ imaging, though, at slightly lower resolution (0.5-2~mm). [11.16,17]

4. Discussion

Serial histological sectioning fills a need to 3D print small anatomical structures that are µm to mm in size and require high spatial resolution. In most previous works introducing methods to 3D print anatomy, intact imaging approaches, especially CT, are used to generate images. Using segmentation approaches, whole systems (such as the airways or vasculature of the lungs), or even whole organs (such as the kidney, liver, or heart), of multi-cm lengthscale and sub-mm-resolution are isolated and printed. [11,16,17] These models have demonstrated value in patient education and visualization of whole-organ structures. However, there is a gap of methodologies capable of 3D printing smaller, µm-scale structures for biological research and educational applications. Here, we show that 3D datasets constructed from serial histological images can fill this niche.

An added benefit of 3D printing structures from serial histological datasets is the ability to detect structures that are too small or too similar in terms of density to be specifically segmented from CT or other intact imaging approaches. Some structures identifiable in H&E, such as PanIN lesions, are too small to be seen directly in low resolution CT images; what's more, they can't be independently labelled with antibodies for visualization through high resolution techniques such as light sheet microscopy of cleared tissues. Unlike CT, which creates 3D images by measuring the density of the target object, or MRI, that images by measuring the release of energy by protons, histological images stained with H&E label nuclei, cytoplasm, and stromal fibers based on the pH of the target tissue. Through H&E staining, basophilic components, such as the DNA inside cellular nuclei, stain a dark blue; and acidophilic components, such as collagen fibers, smooth muscle fibers, and molecules within the cytoplasm of cells, stain a light pink. Thus, observors can visually differentiate microanatomical components including individual epithelial cells, microvasculature, and cancer cells in H&E images that may not be differentiable in CT, MRI, or using antibody targeting.

Here, we show that through segmentation of pancreatic anatomy in registered, serial histological images, we can create anatomically-accurate 3D prints of microscopic pancreatic ducts, precursor lesions, and cancers. CODA fills an important niche where structures of medium size (mm 3 to cm 3 dimensions) and microscopic (cellular or μ m-scale) detail must be 3D printed.

The created models of normal pancreatic ducts, PanINs, and PDACs are significant improvements on current methods of visualizing the complex microanatomy of the pancreas. Most commonly, these structures are viewed in 2D via histological sectioning. 3D reconstruction techniques allow digital 3D visualization of these structures, but the details of these complex structures are limited when seen through a computer screen. 3D printing is a valuable means of communicating these complex structures to wide audiences interested in the development of pancreatic cancer.

Supporting Information

Supporting Information is available from the Wiley Online Library or from the author.

Acknowledgements

The authors would like to thank Chris Gunther from the Johns Hopkins University Whiting School of Engineering Manufacturing for assisting with the 3D printing of the parts shown in this manuscript. The authors acknowledge the following sources of support: U54CA268083; UG3CA275681; Rolfe Pancreatic Cancer Foundation; Lustgarten Foundation-AACR Career development award for pancreatic cancer research in honor of Ruth Bader Ginsburg; The Carl and Carol Nale Fund for Pancreatic Cancer Research; Susan Wojcicki, and Denis Troper.

Conflict of Interest

The authors declare no conflict of interest.

Author Contributions

A.L.K., P.W., and D.W. designed the project. A.L.K., A.F., R.S., and K.S.H. developed the 3D printing workflow. A.L.K. validated the 3D printing workflow. R.H.H. and L.D.W. assisted in histological interpretation. A.L.K., P.W., and D.W. wrote the first draft of the manuscript, which all authors edited and approved.

Data Availability Statement

3D print files are publicly available on the Johns Hopkins University Kiemen laboratory website.

Keywords

3D printing, CODA, deep learning, pancreatic cancer

Received: November 3, 2023 Revised: January 1, 2024 Published online: www.advancedsciencenews.com

www.advmattechnol.de

- [1] R. L. Siegel, K. D. Miller, N. S. Wagle, A. Jemal, CA-Cancer J. Clin. 2023, 73, 17.
- [2] L. Rahib, B. D. Smith, R. Aizenberg, A. B. Rosenzweig, J. M. Fleshman, L. M. Matrisian, *Cancer Res.* 2014, 74, 2913.
- [3] O. Basturk, S. M. Hong, L. D. Wood, N. V. Adsay, J. Albores-Saavedra, A. V. Biankin, L. A. A. Brosens, N. Fukushima, M. Goggins, R. H. Hruban, Y. Kato, D. S. Klimstra, G. Kloppel, A. Krasinskas, D. S. Longnecker, H. Matthaei, G. J. A. Offerhaus, M. Shimizu, K. Takaori, B. Terris, S. Yachida, I. Esposito, T. Furukawa, NIH Public Access 2015, 39 1730
- [4] P. E. Oberstein, K. P. Olive, Ther. Adv. Gastroenterol. 2013, 6, 321.
- [5] R. H. Hruban, M. M. Gaida, E. Thompson, S. M. Hong, M. Noe, L. A. A. Brosens, M. Jongepier, G. Johan, A. Offerhaus, L. D. Wood, Why is pancreatic cancer so deadly?, John Wiley & Sons, Ltd, 2019, 248, pp. 131–141
- [6] C. Koyuncu, A. Janowczyk, X. Farre, T. Pathak, T. Mirtti, P. L. Fernandez, L. Dons, N. P. Reder, R. Serafin, S. S. L. Chow, V. S. Viswanathan, A. K. Glaser, L. D. True, J. T. C. Liu, A. Madabhushi, Laboratory Investigation 2023, 103.
- [7] A. Forjaz, E. Vaz, V. M. Romero, S. Joshi, A. M. Braxton, A. C. Jiang, K. Fujikura, T. C. Cornish, S. M. Hong, R. H. Hruban, P.-H. Wu, L. D. Wood, A. L. Kiem en, D. Wirtz, bioRxiv 2023.
- [8] A. L. Kiemen, A. I. Damanakis, A. M. Braxton, J. He, D. Laheru, E. K. Fishman, P. Chames, C. Almagro-Perez, P.-W. Wu, D. Wirtz, L. D. Wood, R. H. Hruban, *Med* 2023.
- [9] S.-M. Hong, D. Jung, A. Kiemen, M. M. Gaida, T. Yoshizawa, A. M. Braxton, M. Noë, G. Lionheart, K. Oshima, E. D. Thompson, R. Burkhart, P.-H. Wu, D. Wirtz, R. H. Hruban, L. D. Wood, *Mod. Pathol.* 2020, 33, 639.
- [10] P. Tack, J. Victor, P. Gemmel, L. Annemans, *Biomed. Eng. Online* 2016, 15, 115.
- [11] J.-C. Bernhard, S. Isotani, T. Matsugasumi, V. Duddalwar, A. J. Hung, E. Suer, E. Baco, R. Satkunasivam, H. Djaladat, C. Metcalfe, B. Hu, K. Wong, D. Park, M. Nguyen, D. Hwang, S. T. Bazargani, A. L. De Castro Abreu, M. Aron, O. Ukimura, I. S. Gill, World J. Urol. 2016, 34, 337
- [12] R. Javan, D. Herrin, A. Tangestanipoor, Acad. Radiol. 2016, 23, 1183.
- [13] S. V. Murphy, A. Atala, Nat. Biotechnol. 2014, 32, 773.
- [14] E. Mirdamadi, J. W. Tashman, D. J. Shiwarski, R. N. Palchesko, A. W. Feinberg, ACS Biomater. Sci. Eng. 2020, 6, 6453.

- [15] L. Pugliese, S. Marconi, E. Negrello, V. Mauri, A. Peri, V. Gallo, F. Auricchio, A. Pietrabissa, *Updates Surg.* 2018, 70, 381.
- [16] E. R. Perica, Z. Sun, J. Digit. Imaging 2018, 31, 692.
- [17] C. Song, J. H. Min, W. K. Jeong, S. H. Kim, J. S. Heo, I. W. Han, S. H. Shin, S. J. Yoon, S.-Y. Choi, S. Moon, Eur. Radiol. **2023**, *33*, 7646.
- [18] M. Noë, N. Rezaee, K. Asrani, M. Skaro, V. P. Groot, P.-H. Wu, M. T. Olson, S.-M. Hong, S. J. Kim, M. J. Weiss, C. L. Wolfgang, M. A. Makary, J. He, J. L. Cameron, D. Wirtz, N. J. Roberts, G. J. A. Offerhaus, L. A. A. Brosens, L. D. Wood, R. H. Hruban, Am. J. Pathol. 2018, 188, 1530.
- [19] M. Hahn, C. Nord, O. Franklin, T. Alanentalo, M. I. Mettävainio, F. Morini, M. Eriksson, O. Korsgren, M. Sund, U. Ahlgren, Sci. Rep. 2020, 10, 18246.
- [20] A. L. Kiemen, A. M. Braxton, M. P. Grahn, K. S. Han, J. M. Babu, R. Reichel, A. C. Jiang, B. Kim, J. Hsu, F. Amoa, S. Reddy, S.-M. Hong, T. C. Cornish, E. D. Thompson, P. Huang, L. D. Wood, R. H. Hruban, D. Wirtz, P.-H. Wu, *Nat. Methods* 2022, *19*, 1490.
- [21] A. M. raxton, A. L. K Kiemen, M. P. Grahn, A. Forjaz, J. M. Babu, L. Zheng, L. Jiang, H. Cheng, Q. Song, R. Reichel, S. Graham, A. I. Damanakis, C. G. Fisher, S. Mou, C. Metz, J. Granger, X. X. D. X Liu, N. Bachmann, C. Almagro-Perez, A. C. Jiang, J. Yoo, B. Kim, S. Du, E. Foster, J. Y. Hsu, P. Andreu-Rivera, L. C. Chu, F. Liu, N. Niknafs, E. Fishman, A. I, N. J. Roberts, E. D. Thompson, R. B. Scharpf, T. C. Cornish, Y. Jiao, R. Karchin, R. H. Hruban, P. H. Wu, D. Wirtz, L. D. Wood, biorxiv, under review 2023.
- [22] A. L. Kiemen, Y. Choi, A. M. Braxton, C. Almagro-Perez, S. Graham, M. P. Grahn, N. Nanda, N. Roberts, L. Wood, P.-H. Wu, R. H. Hruban, D. Wirtz, *Histopathology* 2022.
- [23] A. T. F. Bell, J. T. Mitchell, A. L. Kiemen, K. Fujikura, H. Fedor, B. Gambichler, A. Deshpande, P. H. Wu, D. N. Sidiropoulos, R. Erbe, J. Stern, R. Chan, S. Williams, J. M. Chell, J. W. Zimmerman, D. Wirtz, E. M. Jaffee, L. D. Wood, E. J. Fertig, L. T. Kagohara, bioRxiv: Cold Spring Harbor Laboratory 2022:2022.07.16.500312.
- [24] A. L. Kiemen, P. H. Wu, A. M. Braxton, T. C. Cornish, R. H. Hruban, L. D. Wood, D. Wirtz, D. Zwicker, bioRxiv 2023.
- [25] A. Deshpande, M. Loth, D. N. Sidiropoulos, S. Zhang, L. Yuan, A. T. F. Bell, Q. Zhu, W. J. Ho, C. Santa-Maria, D. M. Gilkes, S. R. Williams, C. R. Uytingco, J. Chew, A. Hartnett, Z. W. Bent, A. V. Favorov, A. S. Popel, M. Yarchoan, A. Kiemen, P.-H. Wu, K. Fujikura, D. Wirtz, L. D. Wood, L. Zheng, E. M. Jaffee, R. A. Anders, L. Danilova, G. Stein-O'brien, L. T. Kagohara, E. J. Fertig, Cell Syst. 2023, 14, 722.
- [26] Sven. In: inpolyhedron.m, ed: MATLAB central File Exchange, 2023.